Journal of Materials Chemistry A

Accepted Manuscript

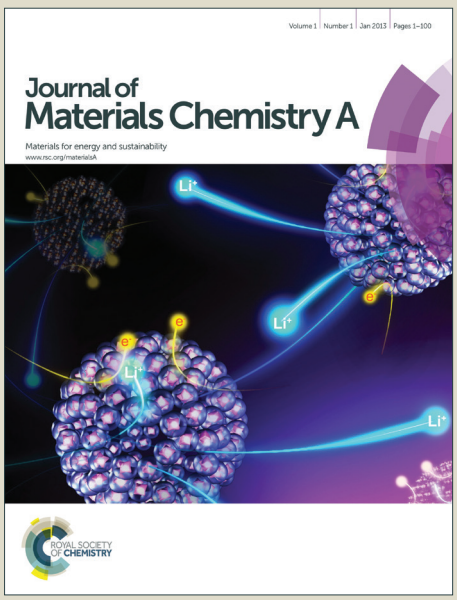

ROYAL SOCIETY OF CHEMISTRY

www.rsc.org/materialsA

Journal Name

ARTICLE

Targeted Synthesis of core-shell Porous Aromatic Frameworks for Selective Detection of Nitro Aromatic Explosives via Fluorescence Two-Dimensional Response

Received 00th January 20xx,
Accepted 00th January 20xx

DOI: 10.1039/x0xx00000x

www.rsc.org/

Heping Ma,[a] Bin Li,[a]* Liming Zhang [a], Dong Han [a] and Guangshan Zhu[b]

A series of core-shell porous aromatic frameworks (PAFs) are synthesized for selective detection of nitro-explosives. The conjugated core-shell PAFs possess large surface area, which can facilitate the pre-concentration of a targeted analyte, leading to superior sensitivity. The tunable LUMO energy levels of these core-shell PAFs make them selectively detecting high explosive TNT and TNP from other competing nitro compounds. Moreover, vapor phase detection of nitro aromatics for PP_C-PPy_S-PAF-2 exhibits a two dimensional fluorescence signal response toward different nitro aromatics. The power to accurately recognize nitro aromatic explosives in fluorescent 2D map highlights the core-shell PAFs as very promising materials for nitro explosive sensing.

1. Introduction

Detection of life-threatening explosives is crucial for military endeavors, national security, criminal investigations as well as for environment and human health.[1] Recent rise in global terrorism has required that the methods for detecting explosives should be sensitive, low-cost and miniaturized. Fluorescent sensing has emerged as a desirable approach for many sensing applications because of its potential for high sensitivity, rapidity of analysis, portability, and cost-effectiveness.[2] Utilizing luminescent materials, effective detection of many high explosive or explosive-like molecules can be achieved by changing of their optical signals.[3] Numerous electron-rich fluorescent conjugated polymers,[4] dyes,[5] fluorescent organic cages,[6] quantum dots[7] and metal organic frameworks (MOFs)[8] have been used in the detection of trace amount of nitro aromatics, which are typically based on fluorescence quenching.

However, solely monitoring the change in emission intensity of luminescent materials can only identify analytes of different categories. For instance, electron deficient molecules as a group can act as fluorescent quenchers. It is still insufficient for accurate and selective detection of one specific electron deficient molecule in their mixture. Upon introducing the change of emission wavelength into detection map, it can add a new variable of fluorescence signal transduction: from one-dimension (emission intensity) to two-dimensions (both fluorescence intensity and wavelength), which may be an effective method to identify one specific molecule in the presence of others.[9] The pioneering work of Li et al. has demonstrated the potential application of luminescent MOFs for explosives detection by fluorescence two-dimensional map.[9,10] Strong analyte-MOF framework interactions are essential to generate a fluorescence signal change both in fluorescence intensity and wavelength. However, moisture sensitive nature of these MOFs may hinder them in practical application.

Porous aromatic framework (PAF), as a new class of nanopore materials, have been demonstrated as a frontier research theme in porous materials. The versatile organic moieties in PAFs make them considerable promising materials in gas adsorption,[11] sensing,[12] photoconductive devices[13] and heterogeneous catalysis,[14]etc. Conjugated PAFs are attractive materials with π-conjugation properties that allow for the detection of various chemicals. Several porous luminescent PAFs have exhibited fast detection for nitroaromatic explosives via fluorescence quenching.[15] Due to their insufficiency excitation-emission center in the skeleton, it is difficult to realize fluorescence two-dimensional (2D) detection in these PAFs. Herein we report the first example of conjugated core-shell porous aromatic frameworks (PAFs) to achieve fluorescent 2D detection of nitroaromatic explosives. The core-shell PAFs possess: (1) large surface areas, which can facilitate the pre-concentration of a targeted analyte, leading to superior sensitivity; (2) two different chromophores in the core and the shell respectively, which can realize both fluorescence intensity and wavelength change in the nitro aromatic explosives detection.

[a] State Key Laboratory of Luminescence and Applications, Changchun Institute of Optics Fine Mechanics and Physics, Chinese Academy of Sciences, Changchun 130033, PR China E-mail: (lib020@ciomp.ac.cn)
[b] Faculty of Chemistry, Northeast Normal University, Changchun 130024, P. R. China.

† Footnotes relating to the title and/or authors should appear here.
Electronic Supplementary Information (ESI) available: [details of any supplementary information available should be included here]. See DOI: 10.1039/x0xx00000x

2. Results

2.1. Synthesis and characterization of PAFs

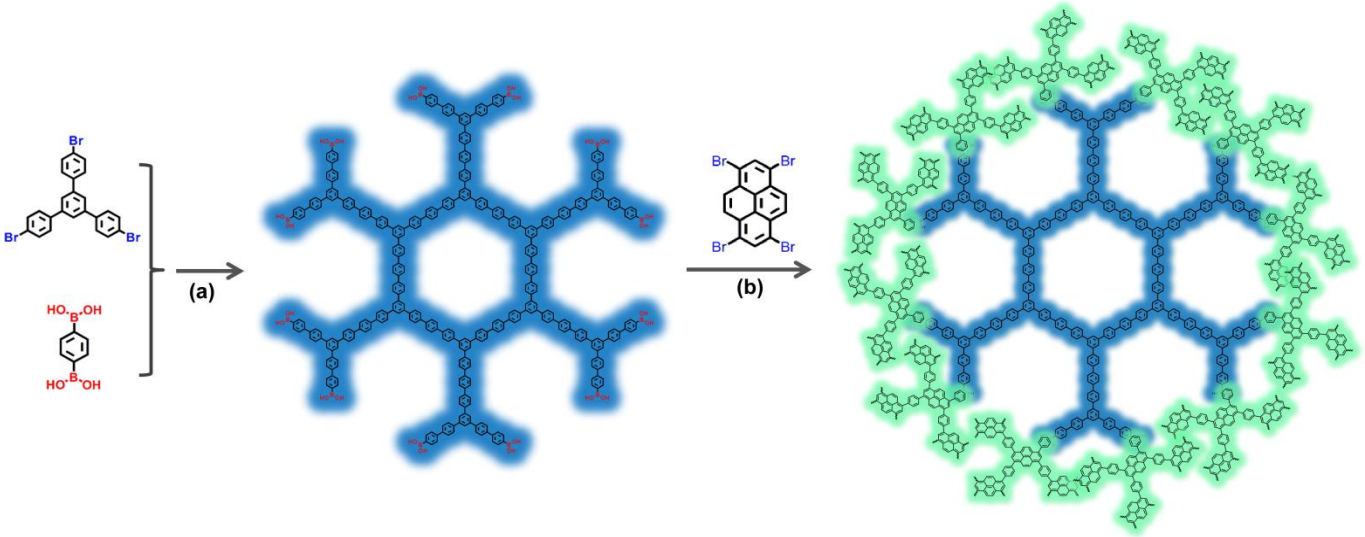

Figure 1. Schematic representation of the synthesis of core-shell PAFs. (a) K_2CO_3 and $Pd(PPh_3)_4$ in DMF, 90 °C, 12h; (b) K_2CO_3 and $Pd(PPh_3)_4$ in DMF, 120 °C, 2d.

We employed a blue emitting polyphenylene PAF (PP-PAF) as a core and polypyrene PAF (PPy-PAF) as a shell to construct core-shell PAFs. The synthetic scheme for this core-shell PAFs networks is shown in Figure 1. PP-PAF core was synthesized by the Suzuki cross-coupling reaction of benzene-1,4-diboronic acid (BDBA) with 1,3,5-Tris(4-bromophenyl)benzene (TBrPB). We used an excess amount of BDBA during core synthesis, which endcapped the core exterior surface of phenylboronic acid functionalities. Phenylboronic acid groups were then reacted with 1,3,6,8-tetrabromopyrene (TBrPy) for shell formation, which ensured shell growth on the exterior surface of core.[16] Changing the TBrPB/TBrPy molar ratio from 8 to 4 and 2 yielded PAFs with three different core-shell composition named: PP_C-PPy_S-PAF-1, PP_C-PPy_S-PAF-2 and PP_C-PPy_S-PAF-3, respectively. As a comparison, we also prepared PP-PAF and PPy-PAF, with TBrPB/TBrPy and BDBA at a molar ratio of 3:1, respectively.

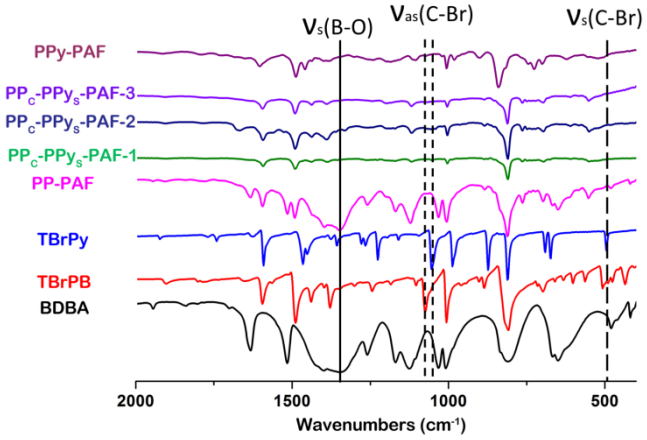

Figure 2. FT-IR spectra of starting monomers and as-prepared PAFs.

All above mentioned polymers were insoluble in common organic solvents such as DMF, THF, methanol, DMSO and water. As found for other phenyl connected porous organic frameworks,[17] these PAFs were also chemically stable: for example, PP_C-PPy_S-PAFs kept their skeleton unchanged even in aqueous solutions of 3M HCl and NaOH for one week.

The PAF samples are first studied by FT-IR spectroscopy and solid-state ^{13}C cross-polarization magic-angle spinning (CP/MAS) NMR. The IR spectra of as-prepared PAFs and their starting monomers are shown in Figure 2. The IR bands corresponding to stretching vibrations of B-O group (1342 cm^{-1}) in PP-PAF core are similar to those of its monomer BDBA, which means that B-O groups are covered on the core. The disappearance of signal assigned to B-O units in all core-shell PAFs demonstrates thatcore is covalently covered by shell. Meanwhile, the IR bands related to C-Br vibration mode at 1072 cm^{-1} and 507 cm^{-1} in TBrPy monomer vanish into the background in all core-shell PAFs, which gives a distinct proof for the complete reaction between core and shell. PP-PAF and PP_C-PPy_S-PAF-2 were further characterized by solid-state ^{13}C CP/MAS NMR (Figure S1). The broad peaks at approximately 147 ppm and 133 ppm are detected, corresponding to substituted aromatic carbon and non-substituted aromatic carbon respectively, which indicates that both PAF framework is composed of highly conjugated aromatic groups. A NMR signal around 127.1 ppm (assigned to the carbon atom in aromatic boronic acid) is observed in PP-PAF, which indicates that PP-PAF core is covered by C-B units. Thermal stability of the PAFs is studied by TGA (Figure S2). A distinct weight loss in the range of 300-400 °C is observed, which corresponds to the decomposition or collapse of the organic skeleton. X-ray photoelectron spectroscopy (XPS) was utilized to determine the purity of our product. The XPS spectra of PP_C-PPy_S-PAF-2 are shown in Figure S3. As can be seen, the main element observed in the polymer network is C element. The low signals from Br, Pd, and N in magnified views of XPS spectra indicate that trace residues of monomers, catalysts, and DMF in final

sample. Powder X-ray diffraction (PXRD) measurement indicates that all PAFs are amorphous (Figure S4). Scanning electron microscopy (SEM) shows that as pyrene shell grows, the particle sizes are increased (Figure S5).

2.2. Porosity of PAFs

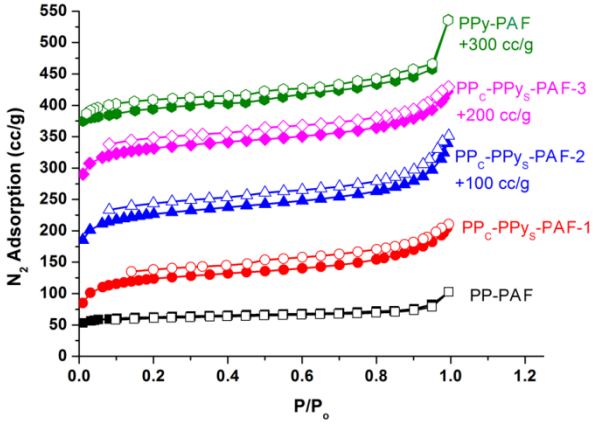

Figure 3. N_2 adsorptiondesorption isotherms measured at 77 K for the PAFs; the adsorption branch is denoted by closed symbols, and desorption branch by open symbols.

The porosity of these PAFs was investigated by nitrogen adsorption and desorption measurement at 77 K. As shown in Figure 3, a sharp increase in gas uptake is observed at low pressure in adsorption-desorption isotherms of PP-PAF, which confirms the existence of micropores in PAF. The Brunauer-Emmett-Teller (BET) surface area of PP-PAF is 265 m^2/g. A weak hysteretic shoulder in desorption isotherms of PP$_C$-PPy$_S$-PAFs prove that these core-shell materials feature a small degree of mesoporosity. The BET surface area is increasing as shell thickness increases. PP$_C$-PPy$_S$-PAF-1 has a BET surface area of 388 m^2/g, while BET surface areas are increased to 402 and 415 m^2/g for PP$_C$-PPy$_S$-PAF-2 and PP$_C$-PPy$_S$-PAF-3, respectively.

2.3 Photophysical property

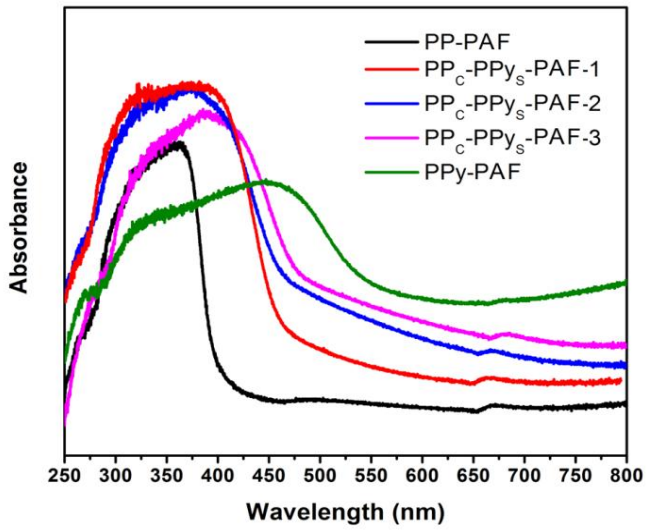

Figure 4. UV-visible absorption spectra of the PAFs measured in the solid state.

The solid UV-visible absorption spectra were used to monitor how π-conjugated network developed during shell growing. As shown in Figure 4 and Figure S6b, PP-PAF core exhibits an absorption band at 400 nm. PP$_C$-PPy$_S$-PAF-1 sample exhibits a red-shifted absorption band at 458 nm. As PPy$_S$-PAF shell network become thicker, the absorption bands are further red-shifted to 460 and 470 nm for PP$_C$-PPy$_S$-PAF-2 and PP$_C$-PPy$_S$-PAF-3, respectively. These data show that it is possible to tune the optical band gaps of core-shell porous networks by adjusting core-shell ratio.

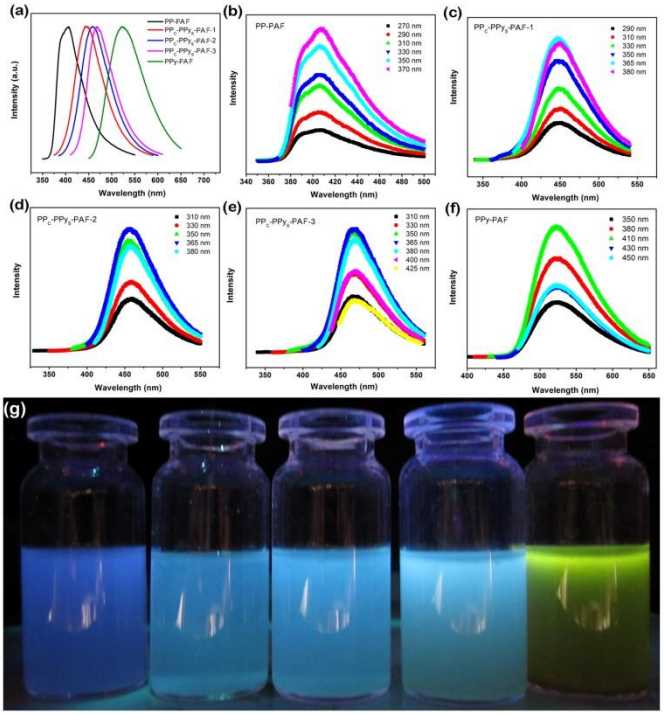

Figure 5. a) Photoluminescence spectra of the PAFs measured in ethanol. A redshift is observed as the pyrene shell incorporation is increased; b-f) The excitation-independent PL behavior of PAFs; g) Photographs of suspensions of the PAFs in ethanol (5mg/10 mL) imaged under irradiation with UV light (λ excitation=365 nm).

Photoluminescence spectra of these PAFs in ethanol solution are given in Figure 5a, while excitation spectra are shown as Figure S6a. Upon excitation of 310 nm in EtOH, PP-PAF core emits a deep-blue luminescence at 409 nm. PPy-PAF exhibits a 525 nm emission upon exciation of 365 nm. Along with the pyrene shell become thicker, a red shift emission is observed, which indicating extended π-electronic conjugation over the PAF skeleton. PP$_C$-PPy$_S$-PAF-1 shows an emission maximum at 452 nm, while PP$_C$-PPy$_S$-PAF-2 gives a luminescence centered at 455 nm. The emission band is further red-shifted to 459 nm for PP$_C$-PPy$_S$-PAF-3. Moreover, PL maxima of PP$_C$-PPy$_S$-PAFs are well confined and independent of excitation wavelength (Figure 5b-5f). We also investigate the PL quantum yield (QY) variation of core-shell PAFs (table S1). PP-PAF shows an absolute QY of 0.1. PP$_C$-PPy$_S$-PAF-1 with a thin shell exhibits a QY value (0.1) similar to that of PP-PAF core. As the shell became thicker, PP$_C$-PPy$_S$-PAFs show enhanced luminescence: the QYs for PP$_C$-PPy$_S$-PAF-2 and PP$_C$-PPy$_S$-PAF-3 are 0.13 and 0.17 respectively.

2.4 Fluorescence response of nitro aromatics in solution

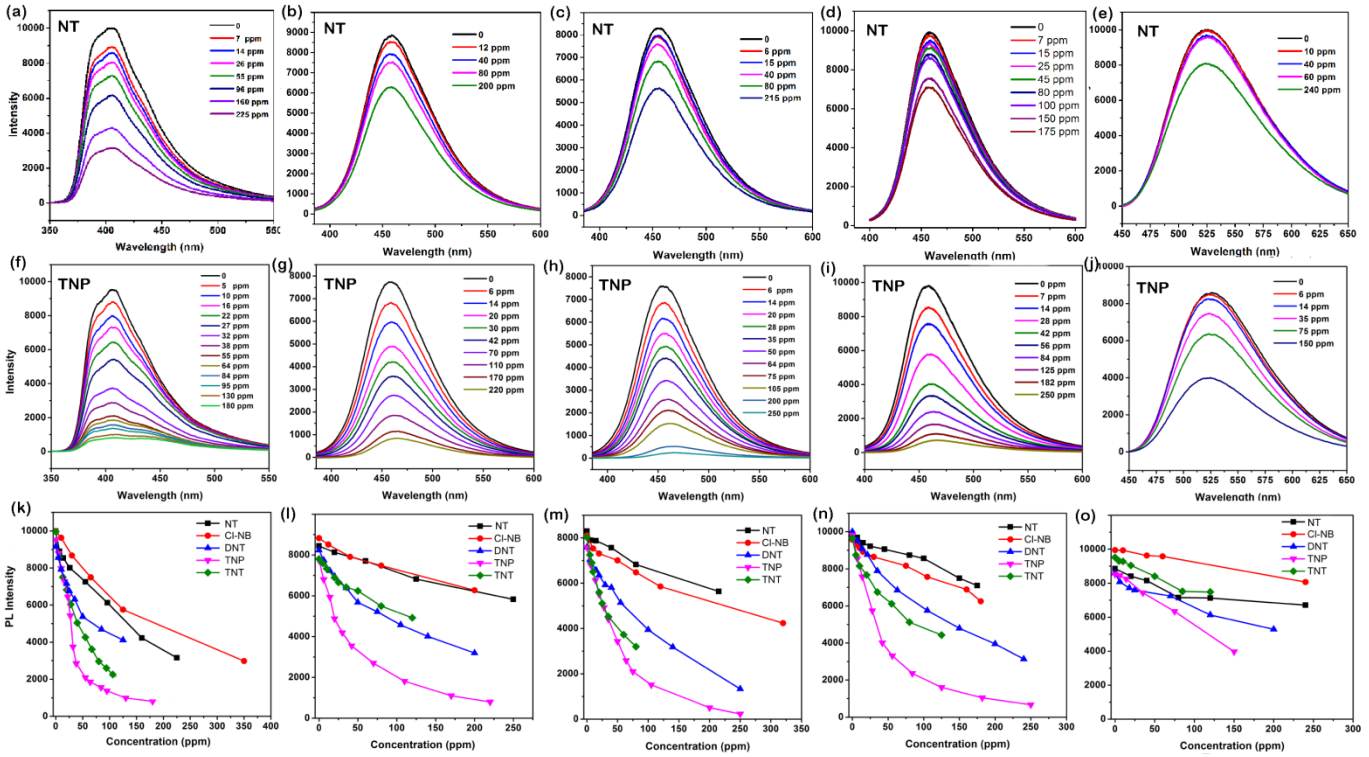

Figure 6. a-e) Effect on the emission spectra of PAFs dispersed in ethanol upon incremental addition of a NT solution, a) for PP-PAF, b) for PP_C-PPy_S-PAF-1, c) for PP_C-PPy_S-PAF-2, d) for PP_C-PPy_S-PAF-3, e) for PPy-PAF; f-j) Effect on the emission spectra of PAFs dispersed in ethanol upon incremental addition of a TNP solution, f) for PP-PAF, g) for PP_C-PPy_S-PAF-1, h) for PP_C-PPy_S-PAF-2, i) for PP_C-PPy_S-PAF-3, j) for PPy-PAF; k-o) Decrease in PAFs fluorescence intensity upon the addition of ethanol solutions of different nitro compounds, k) for PP-PAF, l) for PP_C-PPy_S-PAF-1, m) for PP_C-PPy_S-PAF-2, n) for PP_C-PPy_S-PAF-3, o) for PPy-PAF.

High PL performance and the porous nature of the PAFs inspire us to evaluate their nitro aromatics detection property. p-Nitrotoluene (NT), 4-chloro-nitrobenzene (Cl-NB), 2,4-dinitrotoluene (DNT), 2,4,6-trinitrotoluene (TNT) and 2,4,6-trinitrophenol (TNP) are selected as probe molecules to assess the nitroaromatic compound detection properties of the PAFs. We firstly evaluated fluorescence response of these PAFs to nitro aromatics in solution. Fluorescence quenching titrations of different nitro aromatics were performed by adding various analytes to ethanol solutions of PAFs. PL quenching behavior of these PAFs upon addition of various concentrations of NT, TNP, is shown in Figure 6. Other titration plots can be found in Supporting Information (Figure S7-S11). Immediate fluorescence quenching was observed upon adding high explosive nitro aromatic molecules (TNT and TNP). For PP-PAF, its luminescence intensity is largely dependent on the concentration of nitro aromatic explosives. Moreover, quenching degrees of samples with the same PAF structure for different nitro aromatics are clearly different. The ability of quenching efficiency is in accordance with their order of electron deficiency, where electron withdrawing ability of nitro groups present in the nitro aromatics generally followbelow order: TNP>TNT>DNT>Cl-NB>NT. For PP_C-PPy_S-PAF-1, PP_C-PPy_S-PAF-2 and PP_C-PPy_S-PAF-3, the core-shell composition demonstrates a considerably better selectivity towards TNP and TNT compared to that of PP-PAF and PPy-PAF (Figure 6k-6o). Taking PP_C-PPy_S-PAF-2 for example, PP_C-PPy_S-PAF-2 shows very little quenching for Cl-NB, and NT at a concentration of 50 ppm. The emission peak intensity of PP_C-PPy_S-PAF-2 is decreased by 8% and 7% for Cl-NB and NT, respectively. While PP_C-PPy_S-PAF-2 has a 58% quenching after adding TNT and a 62% quenching by adding TNP under the same concentration, respectively. The quenching efficiency was analyzed using the Stern-Volmer equation: $(F_0/F) = K_{sv}[Q]+1$, where F_0 and F are the fluorescence intensities before and after addition of the analyte, respectively, K_{sv} is the quenching constant (ppm^{-1}), and [Q] is the concentration of the analyte. The SV plots for NB, 2-NT, TNT, and TNP were nearly linear at low concentrations (<75 ppm), and subsequently deviated from linearity, The calculated K_{sv} values for TNT and TNP were 2.21×10^{-2} ppm^{-1} and 2.42×10^{-2} ppm^{-1}, respectively, which are greater than Cl-NB (3.17×10^{-3} ppm^{-1}) and NT (2.33×10^{-3} ppm^{-1}). The most analogous quenching efficiency was also observed for PP_C-PPy_S-PAF-1 and PP_C-PPy_S-PAF-3. For pyrene rich PPy-PAF, upon addition of the same amount of nitro aromatic compounds, little effect on fluorescence intensity varition was observed.

To understand the origin of PP_C-PPy_S-PAF-2 high selectivity towards high explosive TNT and TNP, the mechanism of quenching was investigated. Generally, the fluorescence quenching phenomenon can be explained by donor-acceptor electron-transfer mechanism through the interaction between electron-rich PAFs and electron-deficient analytes.[18] The PAFs can be regarded as giant molecules. Similarly their valence and conduction bands can be treated similar to

molecular orbitals (MOs). Upon excitation, an effective electron transfer occurs from PAF's LUMO to analyte's LUMO only if electron-deficient analyte's LUMO lies between LUMO and HOMO levels of the electron-rich PAFs. Therefore, for electron-deficient analytes with stabilized LUMOs, the PAF usually owns a higher LUMO energy level, electron transfer between them becomes thermodynamically favorable, which may result a high quenching efficiency. If LUMO of analyte is higher than that of the PAF, an effective electron transfer will not occur. Corresponding PL quenching phenomenon will be no obvious. We use circle voltammetry (CV) measurement and absorption spectrum to evaluate HOMO and LUMO changing of these core-shell PAF compared to PP-PAF. The onset potential of oxidation for PP-PAF is +1.17 V vs saturated calomel electrode (SCE) (See Figure S12 in Supporting Information). Hence, PP-PAF's HOMO level is estimated as -5.91 eV. Along with the increasing of pyrene content in shell, onset potential of oxidation for PP_C-PPy_S-PAFs is correspondingly increased (Figure S12 and Table S1). The LUMO levels are determined by combining their CV oxidation potentials with their optical energy band gaps. As shown in Figure S6b, PP_C-PPy_S-PAFs exhibit redshift in the UV-visible spectra compared with PP-PAF. The estimated LUMO energy levels of core-shell PAFs are lower than that of PP-PAF (Table S1). This result is consistent with time-dependent density functional theory (TD-DFT) calculations reported previously.[19]

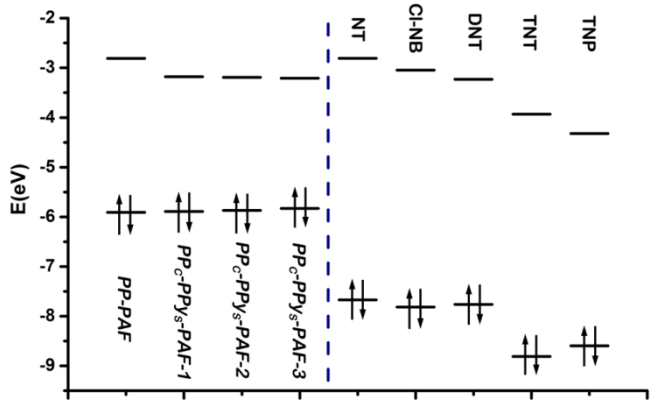

Figure 7. HOMO and LUMO energies for PAFs and analytes arranged in descending order of LUMO energies.

Figure 7 shows the HOMO and LUMO energy levels of these PAFs and electron-deficient nitro compounds as calculated by density functional theory at the B3LYP/6-31G* level (see supporting information and TableS2). The LUMO of PP-PAF is higher than those of all the nitro compounds and thus maintains a better driving force for electron transfer to electron-deficient analytes. So fluorescence quenching was observed for all compounds. Along with the increase of pyrene moiety in the shell, the LUMOs of these PP_C-PPy_S-PAFs were decreased. Since the LUMO energy level of PP_C-PPy_S-PAF-2 is lower than those of Cl-NB and NT, the observed quenching efficiency of PP_C-PPy_S-PAF for Cl-NB and NT is inconspicuous. Thus, PP_C-PPy_S-PAF-2 exhibits selective detection forhigh explosive TNT and TNP from other nitro aromatics.

The high quenching efficiency of PP_C-PPy_S-PAF for TNT in solution (Figure 8a) drives us to testify their selective detection of TNP and TNT for practical application. We dope PP_C-PPy_S-PAF-2 into portable paper-based test strips, which allows a simple and low cost protocol for on-site instant detection. As a comparison, we also dope PP-PAF into a strip in the same way (the detailed method of making test strip is described in supporting information). The resulting test strips display deep-blue photoluminescence (410 nm) for PP-PAF and sky-blue photoluminescence (455 nm) for PP_C-PPy_S-PAF-2 upon exposure to a standard handheld UV (365 nm) lamp, respectively (Figure 8b). To test the sensitivity of these test strips to TNT, different concentrations of TNT solutions (0.25, 5, 10, 15, 20 and 25 mM) were spotted onto the prepared PP_C-PPy_S-PAF-2 strip. Photographs of these test strips after spotted by TNT are shown in Figue 8c. There was visible difference in the quenched spots for the different concentrations of TNT. To further test the application of PP_C-PPy_S-PAF-2 test strip for selective detection of TNP and TNT, we use 100 ppm nitroaromatic compounds ethanol solution as ink and write in PP-PAF and PP_C-PPy_S-PAF-2 strips. As show in Figure 8d, For PP-PAF test strip, when 100 ppm solutions of NT, CL-NB, DNT, TNT and TNP were written onto the strip, its fluorescence was rapidly and almost completely quenched for all compounds. While for PP_C-PPy_S-PAF-2 test strip, only high explosive TNT and TNP quenched the test strip completely. This result showed that the PP_C-PPy_S-PAF-2 test strip is highly sensitive to explosive TNT and TNP with good selectivity.

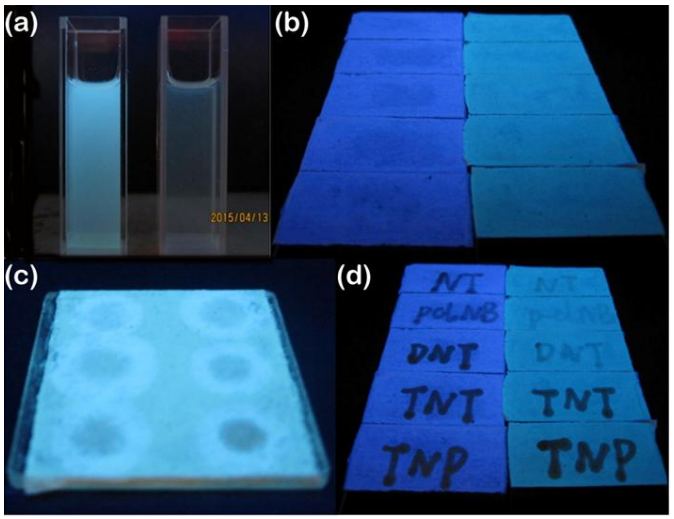

Figure 8. a) Photographs of the original fluorescence and the decreased fluorescence upon addition of TNT in ethanol; b) Photographs of PP-PAF and PP_C-PPy_S-PAF-2 test strips under UV light;c) Photographs of PP_C-PPy_S-PAF-2 test strips after spotting ethanol solution of TNT at different concentrations; d) Photographs of PP-PAF and PP_C-PPy_S-PAF-2 test strips under UV light after writing with 100 ppm solutions of NT, CL-NB, DNT, TNT and TNP.

2.5 Fluorescence response to nitro aromatics vapors

For practical application, we further explore PP_C-PPy_S-PAF for detecting the nitro aromatic in vapor phase. The thick and dense test strips show slow (> 5min) and unspectacular fluorescence quenching response to nitro aromatic (Figure S13). A thin layer of PP_C-PPy_S-PAF-2 was prepared using the method reported by Li etc.[8a] As shown in Figure 9a-9e, fast fluorescence response was observed after exposing PPy_S-PAF-2

towards nitro-compounds vapor for 2 min. Along with the reduction of emission at 455 nm, we also monitor a weak emission around 400 nm for PP_C-PPy_S-PAF-2, which is very similar to PP-PAF core. Utilizing both fluorescence intensity change and emission wavelength shift of PP_C-PPy_S-PAF-2, we can realize fluorescent 2D detection for these nitro-compounds. Fluorescence intensity change and emission wavelength shift of PP_C-PPy_S-PAF-2 for different nitro aromatics are plotted in Figure 9f. These nitro-compounds are well spread on the 2D map and can be uniquely identified. In vapor detection, the nitro compounds only adsorbed on PAF surface, the emission of pyrene shell was quenched effectively. Since the shell layer of PP_C-PPy_S-PAF-2 is very thin, the emission of PP-PAF core can be transmitted through the shell and be detected. This result represents a promising demonstration of nitro aromatics vapor fluorescent 2D detection using core-shell structure PAF. Future studies will focus on preparing novel core-shell PAF so as to increase fluorescent 2D selectivity and sensitivity toward specific class of explosives.

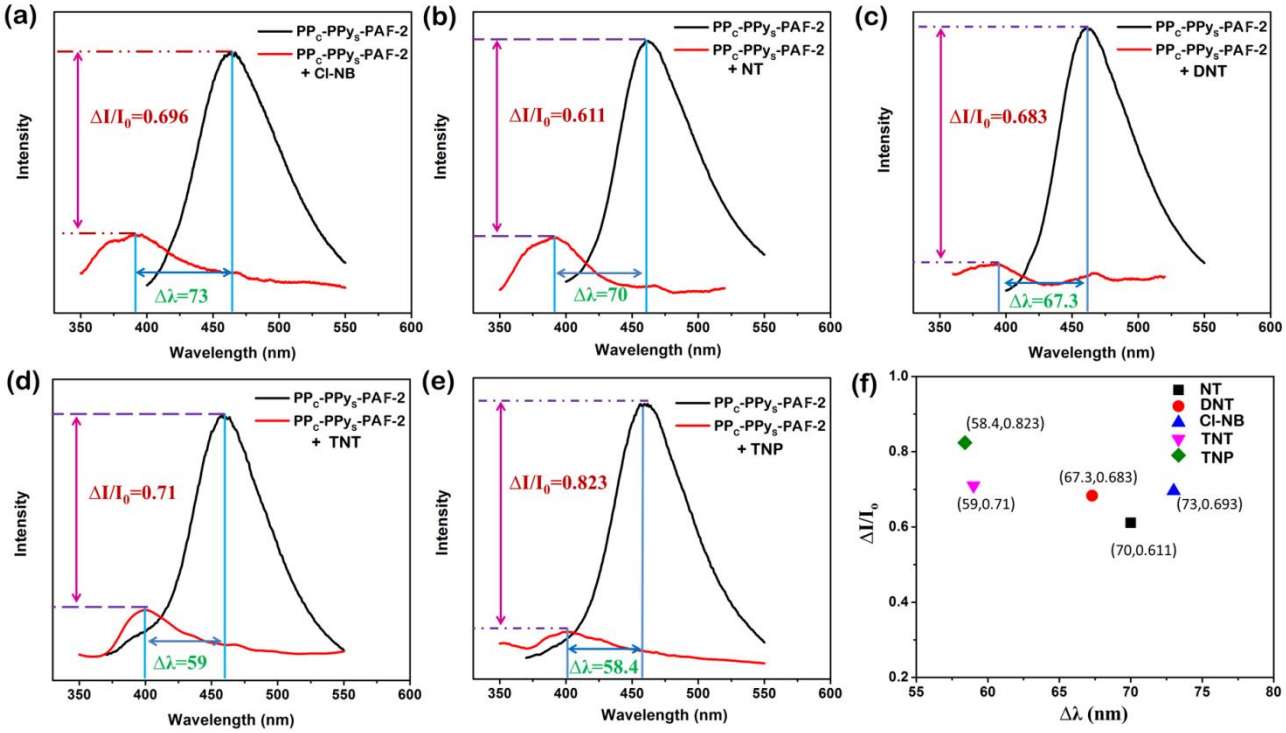

Figure 9. Emission spectra of PP_C-PPy_S-PAF-2 before (black) and after (red) upon exposure to a) Cl-NB, b) NT, c) DNT, d) TNT and e) TNP vapor at room temperature; f) A 2D color coded map of nitro aromatics based on the fluorescence response of PP_C-PPy_S-PAF-2.

3. Conclusions

In conclusion, we have designed and synthesized a series of core-shell conjugated porous aromatic frameworks as fluorescent sensors for the detection of nitro aromatic explosives. The core-shell PAFs exhibited selective detection of high explosive TNT and TNP, over other nitro compounds. Their selectivity can be explained by the decrease of LUMO energy level of the PP_C-PPy_S-PAF after introducing pyrene moiety in shell. Moreover, vapor phase detection of nitroaromatic compound for PP_C-PPy_S-PAF-2 demonstrated the core-shell strategy could achieve fluorescent 2D detection of nitro aromatics. Additionally, because the richness of organic building block could be used to tune their LUMO energy level in the core-shell PAF platform, this very promising approach should be of practical potential for sensitizing and probing different substrate molecules by tuning HOMO-LUMO energy levels. The power to unambiguously recognize nitro aromatic explosives in fluorescent 2D map highlighted this approach as a very promising strategy to develop luminescent core-shell PAF with unprecedented potential applications.

4. Experimental Section

Synthesis of PP-PAF: A mixture of 1,3,5-Tris(4-bromophenyl)benzene (TBrPB) (100 mg, 0.185 mmol), and benzene-1,4-diboronic acid (BDBA) (92 mg, 0.555 mmol) in DMF (15 mL) was degassed by three freeze–pump–thaw cycles. To the mixture was added an aqueous solution of K_2CO_3 (2.0 M, 1.0 mL) and $Pd(PPh_3)_4$ (15.0 mg). The mixture was degassed by three freeze–pump–thaw cycles, and purged with N_2, and stirred at 90 °C for 20 h. The precipitate was filtered, washed with water, methanol, THF, and DMF. Further purification was carried out by Soxhlet extraction with methanol and THF for 48 h, respectively. After dried in a vacuum oven at 150 °C, **PP-PAF** was obtained as grey solid in 85% yield.

Synthesis of PP_C-PPy_S-PAF-1: A mixture of 1,3,5-Tris(4-bromophenyl)benzene (TBrPB) (100 mg, 0.185 mmol), and benzene-1,4-diboronic acid (BDBA) (92 mg, 0.555 mmol) in

DMF (15 mL) was degassed by three freeze–pump–thaw cycles. To the mixture was added an aqueous solution of K_2CO_3 (2.0 M, 1.0 mL) and $Pd(PPh_3)_4$ (15.0 mg). The mixture was degassed by three freeze–pump–thaw cycles, and purged with N_2, and stirred at 90 °C for 12 h. The mixture was allowed to cool at room temperature, and was added with a mixture of 1,3,6,8-tetrabromopyrene (0.023 mmol, 12mg) and catalyst (2 M K_2CO_3, 0.4mL and $Pd(PPh_3)_4$ 9 mg). The resulting mixture was degassed by three freeze–pump–thaw cycles purged with N_2, and stirred at 120 °C for 2 days. The precipitate was filtered, washed with water, methanol, THF, and DMF. Further purification was carried out by Soxhlet extraction with methanol and THF for 48 h, respectively. After dried in a vacuum oven at 150 °C, **PP_C-PPy_S-PAF-1** was obtained as grey solid in 87% yield.

For the synthesis of **PP_C-PPy_S-PAF-2 and PP_C-PPy_S-PAF-3**, the same reaction procedure was performed unless the added with 1,3,6,8-tetrabromopyrene was 0.046 mmol and 0.092 mmol, respectively.

Acknowledgements

The authors gratefully thank the financial supports of the NSFC (Grant Nos. 51172224 and 51372240).

Notes and references

‡ Footnotes relating to the main text should appear here. These might include comments relevant to but not central to the matter under discussion, limited experimental and spectral data, and crystallographic data.

1. a) S. W. Thomas III, G. D. Joly, T. M. Swager, *Chem. Soc. Rev.* 2007, **36**, 1339; b) R. L. Woodfin, *Trace Chemical Sensing of Explosives,* John Wiley & Sons, 2006.
2. R. A. Agbaria, P. B. Oldham, M. McCarroll, L. B. McGown, I. M. Warner, *Anal. Chem.* 2002, **74**, 3952.
3. Y. Salinas, R. Martinez-Manez, M. D. Marcos, F. Sancenon, A. M. Castero, M. Parra, S. Gil, *Chem. Soc. Rev.* 2012, **41**, 1261.
4. a) M. E. Germain, M. J. Knapp, *Chem. Soc. Rev.* 2009, **38**, 2543; b)S. W. Thomas, G. D. Joly, T. M. Swager, *Chem. Rev.* 2007, **107**, 1339.
5. N. Venkatramaiah, A. Firmino, F. A. Almeida Paz, J. P. C. Tome´, *Chem. Commun.* 2014, **50**, 9683.
6. K. Acharyya, P. Sarathi Mukherjee, *Chem. Commun.* 2014, **50**, 15788.
7. a) K. Zhang, H. Zhou, Q. Mei, S. Wang, G. Guan, R. Liu, J. Zhang, Z. Zhang, *J. Am. Chem. Soc.* 2011, **133**, 8424; b) R. Freeman, T. Finder, L. Bahshi, R. Gill, I. Willner, *Adv. Mater.* 2012, **24**, 6416; c) P. Wu, C. Xu, X. Hou, J. Xu, H. Chen, *Chem. Sci.* DOI: 10.1039/C5SC01497B.
8. a) A. Lan, K. Li, H. Wu, D. H. Olson, T. J. Emge, W. Ki, M. Hong, J. Li, *Angew. Chem. Int. Ed.* 2009, **48**, 2334; b) S. S. Nagarkar, B. Joarder, A. K. Chaudhari, S. Mukherjee, S. K. Ghosh, *Angew. Chem. Int. Ed.* 2013, **52**, 2881; c) B. Gole, A. K. Bar, P. S.Mukherjee, *Chem. Eur. J.* 2014, **20**, 13321; d) H. Xu, F. Liu, Y. Cui, B. Chen, G. Qian, *Chem. Commun.* 2011, **47**, 3153; e) S. S. Nagarkar, A. V. Desai and S. K. Ghosh, *Chem. Commun.*, 2014, **50**, 8915; f) J. Qin, B. Ma, X.-F. Liu, H.-L. Lu, X.-Y. Dong, S.-Q. Zang and H. Hou, *J. Mater. Chem. A,* 2015, **3**, 12690.
9. Z. Hu, B. J. Deibert, J. Li, *Chem. Soc. Rev.* 2014, **43**, 5815.
10. a) Z. Hu, S. Pramanik, K. Tan, C. Zheng, W. Liu, X. Zhang, Y. J. Chabal, J. Li, *Cryst. Growth Des.* 2013, **13**, 4204; b) Z. Hu, K. Tan, W. P. Lustig, H. Wang, Y. Zhao, C. Zheng, D. Banerjee, T. J. Emge, Y. J. Chabal, J. Li, *Chem. Sci*. 2014, **5**, 4873.
11. a) R. Dawson, A. I. Cooper, D. J. Adams, *Prog. Polym. Sci.* 2012, **37**, 530; b) X. Q. Zou, H. Ren, G. S. Zhu, *Chem. Commun.* 2013, **49**, 3911.
12. a) X. Liu, Y. Xu, D. Jiang, *J. Am. Chem. Soc.* 2012, **134**, 8738; b) C. Gu, N. Huang, J. Gao, F. Xu, Y. Xu, D. Jiang, *Angew. Chem. Int. Ed.* 2014, **53**, 4850.
13. a) L. Chen, Y. Honsho, S. Seki, D. Jiang, *J. Am. Chem. Soc.* 2010, **132**, 6742; b) K. Zhang, D. Kopetzki, P. H. Seeberger, M. Antonietti, F. Vilela, *Angew. Chem. Int. Ed.* 2012, **52**, 1432; c) X. Feng, X. Ding, D. Jiang, *Chem. Soc. Rev.* 2012, **41**, 6010.
14. a) L. Chen, Y. Yang, Z. Guo, D. Jiang, *Adv. Mater.* 2011, **23**, 3149; b) J. X. Jiang, C. Wang, A. Laybourn, T. Hasell, R. Clowes, Y. Z. Khimyak, J. Xiao, S. J. Higgins, D.J. Adams, A.I. Cooper, *Angew. Chem., Int. Ed.* 2011, **50**, 1072; c) R. K. Totten, Y.-S. Kim, M. H. Weston, O. K. Farha, J. T. Hupp, S. T. Nguyen, *J. Am. Chem. Soc.* 2013, **135**, 11720.
15. a) D. Gopalakrishnan, W. R. Dichtel, *J. Am. Chem. Soc.* 2013, **135**, 8357; b) Y. Yuan, H. Ren, F. Sun, X.Jing, K. Cai, X. Zhao, Y. Wang, Y. Wei, G. Zhu, *J. Phys. Chem. C* 2012, **116**, 26431; c) N. Sang, C. Zhan, D. Cao, *J. Mater. Chem. A*, 2015, **3**, 92.
16. Y. Xu, A. Nagai, D. Jiang, *Chem. Commun.* 2013, **49**, 1591.
17. T. Ben, H. Ren, S. Q. Ma, D. P. Cao, J. H. Lan, X. F. Jing, W. C. Wang, J. Xu, F. Deng, J. M. Simmons, S. L. Qiu, G. S. Zhu, *Angew. Chem. Int. Ed.* 2009, **48**, 9457.
18. D. T. McQuade, A. E. Pullen, T. M. Swager, *Chem. Rev.* 2000, **100**, 2537.
19. R. S. Sprick, J.-X. Jiang, B. Bonillo, S. Ren, T. Ratvijitvech, P. Guiglion, M. A. Zwijnenburg, D. J. Adams, A. I. Cooper, *J. Am. Chem. Soc.*, 2015, **137**, 3265.

The table of contents:

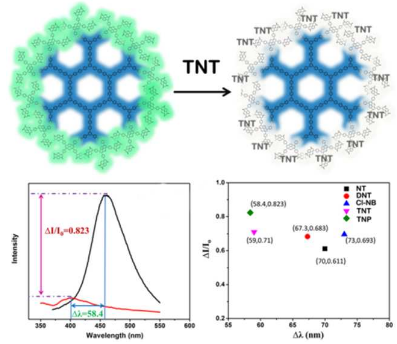

A series of conjugated core-shell porous aromatic frameworks are synthesized for selective detection of nitro-explosives. The core-shell PAFs can recognize nitro aromatic explosives in fluorescent 2D map via both fluorescence intensity and wavelength response.